PHYSICAL REVIEW C **81**, 061603(R) (2010)

Roles of deformation and orientation in heavy-ion collisions induced by light deformed nuclei at intermediate energy

X. G. Cao,[1,2] G. Q. Zhang,[1,2] X. Z. Cai,[1,*] Y. G. Ma,[1] W. Guo,[1] J. G. Chen,[1] W. D. Tian,[1] D. Q. Fang,[1] and H. W. Wang[1]

[1]*Shanghai Institute of Applied Physics, Chinese Academy of Sciences, Shanghai 201800, China*

[2]*Graduate School of the Chinese Academy of Sciences, Beijing 100049, China*

(Received 18 November 2009; published 23 June 2010)

The reaction dynamics of axisymmetric deformed ^{24}Mg + ^{24}Mg collisions has been investigated systematically by an isospin-dependent quantum molecular dynamics model. It is found that different deformations and orientations result in apparently different properties of reaction dynamics. We reveal that some observables such as nuclear stopping power (R), multiplicity of fragments, and elliptic flow are very sensitive to the initial deformations and orientations. There exists an eccentricity scaling of elliptic flow in central body-body collisions with different deformations. In addition, the tip-tip and body-body configurations turn out to be two extreme cases in central reaction dynamical process.

DOI: 10.1103/PhysRevC.81.061603 PACS number(s): 24.10.Cn, 24.70.+s, 25.70.Mn

Aligned experiments investigating how a deformed ^{165}Ho target affects the total neutron reaction cross section from 2 to 125 MeV [1] and scattering of α particles with $15 \leqslant E_\alpha \leqslant 23$ MeV [2] were carried out about 40 years ago. The similar case occurs in nanoscale physics whereby the initial shape of hot droplets also has significant effects on the fragmentation process in the molecular dynamics (MD) framework [3]. It is expected that deformed nuclei-induced heavy-ion collisions (HICs) can result in obviously different properties of dynamical processes and final-state observables compared with spherical cases. There are some reports about deformed $U + U$ collisions at relativistic and ultrarelativistic energies and it is suggested that deformed $U + U$ collisions are more likely to create quark-gluon plasma (QGP) and may resolve many outstanding problems [4–11]. The deformation effects on reaction cross section [12], elliptic flow [13], and heavy-ion fusion [14,15] was also discussed recently. On the other hand, polarized targets and beams have been widely applied related with spin effects in HICs [16], especially for the total and differential reaction cross-section measurements of aligned deformed beams such as ^{7}Li [17] and ^{23}Na [18].

Recently spin-polarized beams have been widely used in projectile-fragmentation reactions [19], which brings large angular momentum into fragment spin. Not only does the fragmentation process itself produce spin-polarized fragments but also the produced spin-orientated beams of deformed nuclei can provide valuable information on shape effects during collisions [20]. Therefore, it is very necessary to consider the degree of freedom of the initial deformation since so many radioactive nuclei far from the β-stability line may have large deformations. However, knowledge about collisions induced by deformed nuclei is very poor, especially at intermediate energies.

Due to the distinct differences in the overlap region of deformed nuclei collisions, collisions of aligned deformed nuclei may give a clearer and deeper insight into the reaction mechanism such as the process of multifragmentation and the development of collective flow. The different orientational collisions also have the advantage in fixing the uncertain behavior of density-dependent symmetry energy, which is an elementary open problem related not only to many problems in nuclear physics but also to a number of important issues in nuclear astrophysics [21]. Besides the advantage in studying reaction mechanism and dynamics, highly deformed nuclei-induced reactions may also inspire exotic nuclei research such as halo [22] and cluster phenomena [23].

In this Rapid Communication, an ^{24}Mg + ^{24}Mg collision system is used to investigate the initial deformation and orientation effects by a microscopic transport model, the isospin-dependent quantum molecular dynamics (IDQMD) model [24], which is developed from the quantum molecular dynamics (QMD) model [25]. The main advantage of the QMD model is that it can explicitly treat the many-body state of collision system. So it contains correlation effects to all orders and can treat the fragmentation and fluctuation of HICs well.

In these calculations, soft and hard nuclear equations of state (EOS) with the incompressibility of $K = 200$ and 380 MeV, respectively, are used for comparison. Here the strength of symmetry potential $C_{\rm sym} = 32$ MeV [25] and an experimental parameterized nucleon-nucleon cross section which is energy and isospin dependent are used. ^{24}Mg is approximately treated as a sharp-cutoff ellipsoid with a large quadrupole deformation parameter: $\beta_2 = 0.416$ [26]. For comparison, systematical calculations for sphere-sphere or tip-tip (body-body) collisions of ^{24}Mg + ^{24}Mg with $\beta_2 = 0$, 0.05, 0.1, 0.2 (all four cases with the same root-mean-square radius) at different energies and impact parameters are carried out. The schematic plot of tip-tip and body-body collisions is illustrated by Fig. 1.

First, we discuss the nuclear stopping power ($R = \frac{2}{\pi}\sum_i^A |P_{i\perp}| / \sum_i^A |P_{i\parallel}|$, where A refers to the sum of projectile mass number and target mass number, $P_{i\perp} = (P_{ix}^2 + P_{iy}^2)^{1/2}$, $P_{i\parallel} = P_{iz}$ in the center-of-mass reference system [27]) for different orientational collisions. R can be used to describe the momentum dissipation and the degree of thermalization. Figure 2(a) shows that central body-body collisions lead to larger R than central tip-tip collisions below 50 MeV/nucleon

*caixz@sinap.ac.cn

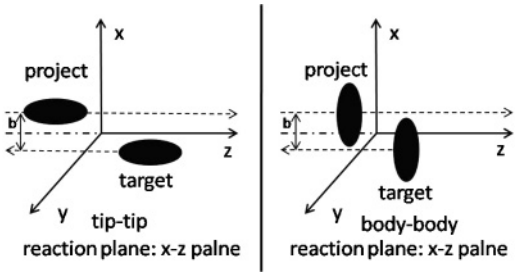

FIG. 1. Schematic representation of tip-tip and body-body collisions. In the coordinate system, the z direction is defined as the incident direction and the impact parameter b is labeled as the x axis. Only b parallel to ^{24}Mg's long axis in body-body collisions is considered.

while the situation is reversed when incident energies exceed 75 MeV/nucleon. If ^{24}Mg is more prolate, then more obvious differences appear. The spherical case lies between the tip-tip and body-body collisions at almost all calculated energies. The larger R of tip-tip collisions at higher energy is in agreement with the result at 0.52 GeV/nucleon with the a relativistic transport (ART) model [10]. However, the inversion of R between the tip-tip and body-body collisions is first observed. It reflects the different roles of the initial space configurations vs. energies.

It is known that the reaction mechanism at intermediate energy is dominated by mean field, binary collisions, and Pauli blocking. Since the IDQMD model can treat the three components explicitly, it is very convenient to find out the factors which dominate the stopping power at different energies. As represented in Figs. 2(b) and 2(c), tip-tip collision numbers are higher than body-body ones at all considered energies. It means that only binary collisions cannot be responsible for the inversion of R, while the mean field must play a very important role. Figure 3 shows how mean field

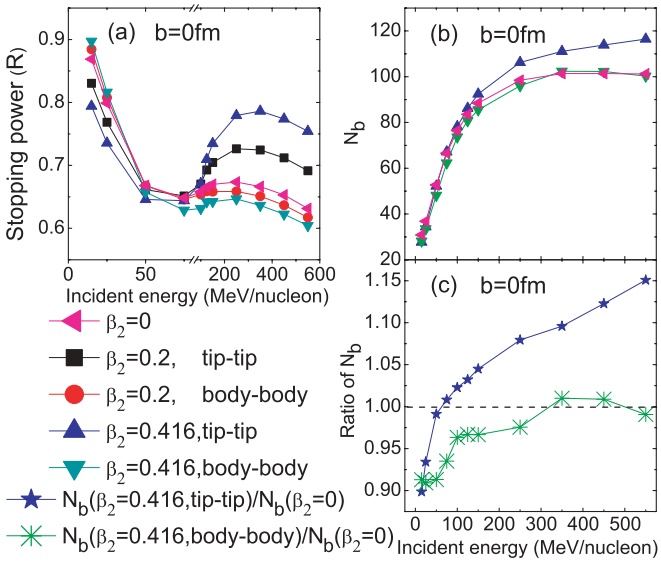

FIG. 2. (Color online) (a) R and (b) total binary collision number (N_b) as a function of incident energy at freeze-out time. (c) The ratio of the nonspherical N_b to the spherical one.

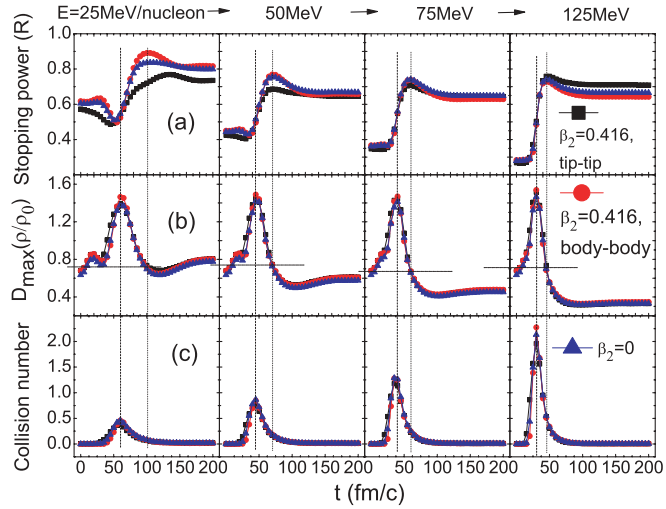

FIG. 3. (Color online) (a), (b), and (c) represent the time evolutions of R, maximal density D_{max}, and N_b in central collisions ($b = 0$ fm), respectively. The long-dashed, short-dashed, and dash-dotted lines are drawn to mark the characteristic time of the collisions. The time structure of the N_b is synchronous with the density evolution. Time evolution of R shows that tip-tip, body-body, and sphere-sphere collisions experience different touching, compressing, and expanding processes from $t = 0$ to the freeze-out stage.

and binary collisions take effect in dynamical process. The peak of density corresponds to the most intensive stopping process but the R has not reached maximum. The departure between projectile-like and target-like continues contributing the nuclear stopping power. Through the different stopping behaviors of tip-tip and body-body collisions vs. energies, the time evolutions of R show that when reaction proceeds more quickly, the larger stopping power can be achieved. So the stopping power can be regarded as a measurement of time scale of dynamical process as well as an observable of momentum dissipation.

Due to the larger projectile-target overlap region, body-body configurations build up stronger mean field, which lead to more violent one-body scattering. However, the transparency effect of the nuclear medium becomes more and more important when incident energy rises. The tip-tip configurations are less transparent, which lead to stronger two-body collisions and larger stopping power. Therefore, the underlying mechanism of the inversion for R between tip-tip and body-body collisions is that body-body configurations build up a stronger mean field at lower energies, where one-body scattering is predominant, whereas two-body collisions become more important in tip-tip configurations at higher energies.

Since the IDQMD model can treat fragmentation of hot nuclei [28,29] well, it is appropriate to investigate the fragmentation observables. As shown in Fig. 4, the fragment multiplicity has strong correlation with stopping power. Body-body collisions have minimal multiplicity at all impact parameters at higher energies while tip-tip collisions have the maximal one. So this behavior is consistent with that of stopping power at higher energies. It can also be seen from charge distributions in Fig. 5 that the tip-tip and body-body

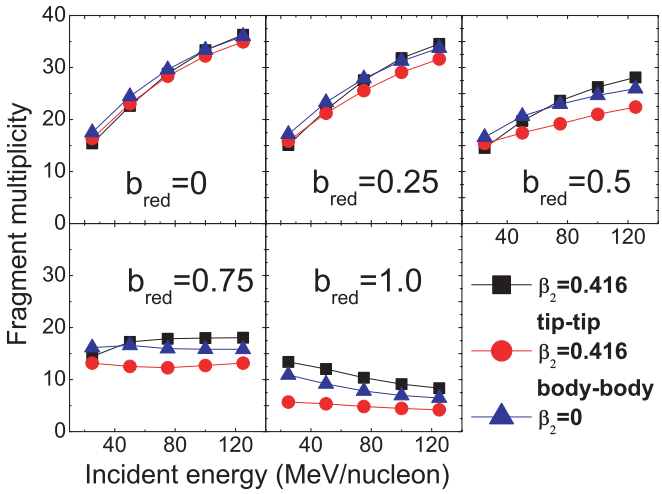

FIG. 4. (Color online) Energy dependence of fragment multiplicity of tip-tip, body-body, and sphere-sphere collisions at different reduced impact parameters ($b_{\rm red} = b/b_{\rm max}$, where $b_{\rm max}$ refers to the maximal impact parameter for different cases).

collisions are two extreme cases and sphere-sphere collisions lie between them. Therefore, the fragment observables also confirm the similar picture indicated by R.

The body-body collisions with $b = 0$ fm will produce large collective motions due to the different initial geometry from spherical nuclei. An anisotropic flow method has been developed to measure the anisotropy of particle momentum space which is related to the nuclear EOS and nuclear reaction dynamics [30–32]. The azimuthal distribution of fragments can be expressed by Fourier expansion [33] $\frac{dN}{d\phi} \propto 1 + 2\sum_{n=1}^{\infty} v_n \cos(n\phi)$, where ϕ is azimuthal angle between the transverse momentum of the particle and the reaction plane. The coefficient v_n is defined as anisotropic flow parameter,

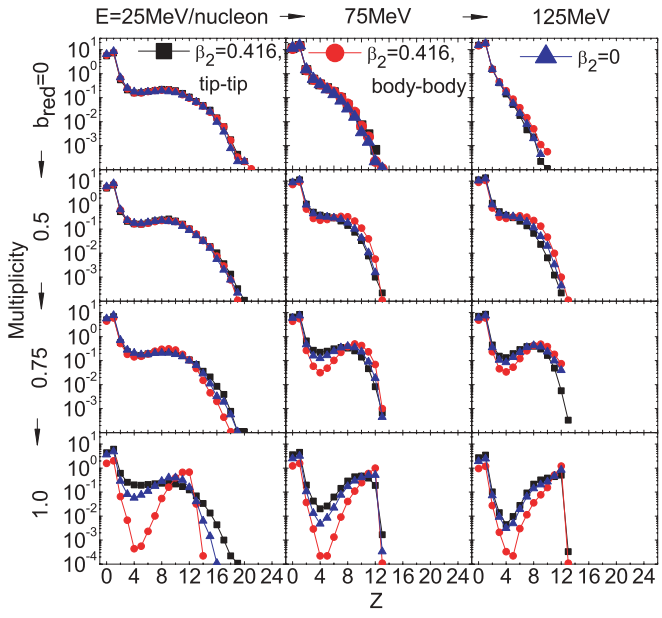

FIG. 5. (Color online) Charge distributions of tip-tip, body-body, and sphere-sphere collisions at different $b_{\rm red}$ and incident energies.

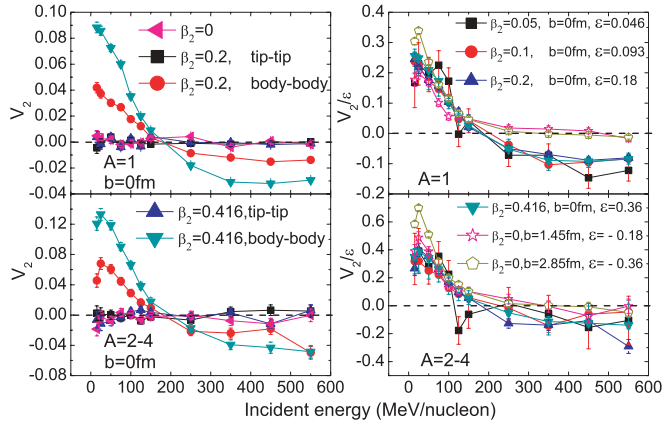

FIG. 6. (Color online) The v_2 excitation function of light fragments at midrapidity ($-0.5 < Y < 0.5$) of deformed and spherical collisions. The dashed lines are drawn to guide the eye. (Left) The v_2 in central collisions with $b = 0$ fm; (right) scaled v_2 with eccentricity ϵ in central body-body collisions and noncentral spherical ^{24}Mg collisions. The spherical ^{24}Mg collisions with $b = 1.45$ fm and 2.85 fm have the same absolute value of ϵ as the deformed central ^{24}Mg collisions with $\beta_2 = 0.2$ and 0.416, respectively.

among which v_2 denotes elliptic flow. It can be calculated in terms of single-particle averages: $v_2 = \langle \cos(2\phi) \rangle = \langle \frac{p_x^2 - p_y^2}{p_x^2 + p_y^2} \rangle$. The nucleon's v_2 induced by deformed $U + U$ collisions has been studied recently using the ART model [5,10] and the optical Glauber model [13] at relativistic energies. It seems that the most central body-body collisions give rise to largest v_2 because of the strongest shadowing effect in the reaction plane [5]. Thus v_2 of central body-body collisions is most appropriate for investigating the nuclear EOS. However, v_2 developing from deformed nuclei collisions is unknown at intermediate energy and it is interesting to study their deformation and orientation effects.

The v_2 of light fragments is shown in Fig. 6, in which the eccentricity (ϵ) is calculated by the maximal geometry overlap region: $\epsilon = \sum_i (x_i^2 - y_i^2) / \sum_i (x_i^2 + y_i^2)$. Cental tip-tip and sphere-sphere collisions do not have obvious v_2 because of the transverse symmetry of overlap region while the v_2 of cental body-body collisions has a nonzero value. The negative sign of v_2 at higher energies is in agreement with deformed $U + U$ collisions by the ART model [5,10]. The positive v_2 at lower energies and the alteration of sign for v_2 are first observed in central body-body collisions. At higher energies the violent two-body collisions in overlap region build the anisotropy pressure and it prompts fragments emission from in-plane preferential to out-of-plane preferential. The heavier fragments have larger v_2, which is consistent with Ref. [34]. The v_2 of central body-body collisions ($\beta_2 = 0.05, 0.1, 0.2, 0.416$) can be scaled together by ϵ from low energies to high energies. While scaled by the same ϵ amplitude as the deformed ^{24}Mg collisions, the v_2 for midcentral spherical ^{24}Mg collisions shows different behaviors, especially for higher energies. Therefore, the scaling of v_2 indicates that the geometric shapes of participants play an essential role in collective flow of central body-body collisions.

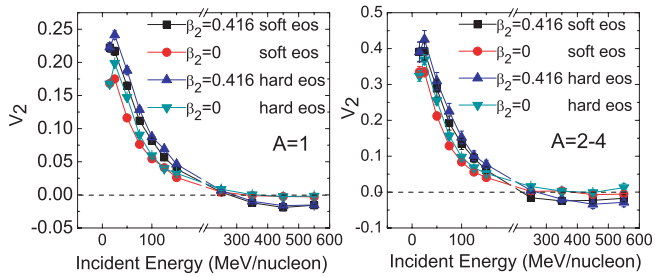

FIG. 7. (Color online) Average v_2 excitation function of light fragments at midrapidity ($-0.5 < Y < 0.5$) for deformed and spherical collisions with soft and hard nuclear EOS. v_2 is averaged with b from 0 to b_{max} for body-body and sphere-sphere collisions.

The energy excitation function of v_2 at midcentral sphere-sphere collisions varies from positive (in-plane, rotational-like emission) to negative (out-of-plane, "squeeze-out" pattern) [31,35]. This energy point is the so-called transition energy, which is near 100 MeV/nucleon [31]. For a spherical collision system, there exist three competing components affecting the transition energy: (i) rotation of the compound system, (ii) expansion of the hot and compressed participant zone, and (iii) shadowing of the colder spectator region [31]. Only the expansion survives in central spherical collisions [36,37], which merely generates azimuthal symmetric flow. However, central body-body collisions have bulk transverse asymmetry overlap region and there is no rotation effect. Moreover, the shadowing differs from midcentral collisions of spherical nuclei. Therefore, it provides an ideal tool to understand how the azimuthal pressure, expansion, and flow develop from the almond-shaped overlap, which are all related with the extraction of the nuclear EOS. Impact parameter average v_2 is shown in Fig. 7 with soft and hard nuclear EOS. The hard nuclear EOS enhances v_2 for both spherical and deformed collisions. Deformed configuration gives rise to larger v_2 than spherical configuration for both soft and hard nuclear EOSs.

In summary, deformed $^{24}\mathrm{Mg} + ^{24}\mathrm{Mg}$ collisions have been studied systematically using the IDQMD model. The inversion of R vs. energies between tip-tip and body-body collisions reflects the two different configurations that play different roles in reaction dynamics. The fragment observables also show different behaviors for the two extreme configurations. The sphere-sphere collisions lie between the tip-tip and body-body collisions in nuclear stopping and fragmentation. Moreover, the excitation functions of v_2 for different deformed central body-body collisions can be scaled on a similar curve by eccentricity. The v_2 averaged by impact parameter (collision configuration is represented by Fig. 1) in deformed collisions is stronger than that of spherical collisions for both soft and hard nuclear EOSs. The large v_2 developed from cental body-body collisions have advantages in studying the nuclear EOS and transition energy. Tip-tip collisions can be used to study the liquid-gas phase transition in finite nuclear systems due to the longer collision time. In addition, deformed nuclei collisions may have some implications on halo and cluster structure research. Therefore, the merits of collisions with deformed nuclei can shed light on the studies of both the nuclear structure and the reaction dynamics from low energies to relativistic energies.

This work is partially supported by National Natural Science Foundation of China under Contract Nos. 10775167, 10775168, 10979074, 10605036, 10875160, 10805067 and 10975174; Major State Basic Research Development Program in China under Contract No. 2007CB815004, the Shanghai Development Foundation for Science and Technology under Contract No. 09JC1416800 and the National Defence Innovation Foundation of Chinese Academy of Sciences under Grants No. CXJJ-216.

[1] H. Marshak *et al.*, Phys. Rev. Lett. **20**, 554 (1968).
[2] D. R. Parks *et al.*, Phys. Rev. Lett. **29**, 1264 (1972).
[3] N. Komatsu and T. Abe, Phys. Rev. E **72**, 021601 (2005).
[4] S. Das Gupta and C. Gale, Phys. Rev. C **62**, 031901(R) (2000).
[5] B. A. Li, Phys. Rev. C **61**, 021903(R) (2000).
[6] E. V. Shuryak, Phys. Rev. C **61**, 034905 (2000).
[7] U. Heinz and A. Kuhlman, Phys. Rev. Lett. **94**, 132301 (2005).
[8] A. Kuhlman and U. Heinz, Phys. Rev. C **72**, 037901 (2005).
[9] C. Nepali, G. Fai, and D. Keane, Phys. Rev. C **76**, 051902(R) (2007).
[10] X. F. Luo *et al.*, Phys. Rev. C **76**, 044902 (2007).
[11] H. Masui *et al.*, Phys. Lett. B **679**, 440 (2009).
[12] J. A. Christley and J. A. Tostevin, Phys. Rev. C **59**, 2309 (1999).
[13] P. Filip, Phys. At. Nucl. **71**, 1609 (2008).
[14] R. G. Stokstad *et al.*, Phys. Rev. Lett. **41**, 465 (1978).
[15] V. Y. Denisov and N. A. Pilipenko, Phys. Rev. C **76**, 014602 (2007).
[16] D. Fick *et al.*, Phys. Rep. **214**, 1 (1992).
[17] K. H. Möbius *et al.*, Phys. Rev. Lett. **46**, 1064 (1981).
[18] N. M. Clarke *et al.*, Phys. Rev. C **47**, 660 (1993).
[19] K. Asahi, Prog. Part. Nucl. Phys. **46**, 321 (2001).
[20] Exploratory Workshop on Polarized Radioactive Beams and Polarized Targets, 6–7 March 2003, Strasbourg, France; [http://wwwires.in2p3.fr/ires/workshops/polar03/].
[21] B. A. Li *et al.*, Phys. Rep. **464**, 113 (2008).
[22] D. Q. Fang *et al.*, Phys. Rev. C **76**, 031601(R) (2007).
[23] M. Freer, Rep. Prog. Phys. **70**, 2149 (2007).
[24] Y. G. Ma *et al.*, Phys. Rev. C **73**, 014604 (2006).
[25] J. Aichelin, Phys. Rep. **202**, 233 (1991).
[26] G. A. Lalazissis *et al.*, At. Data Nucl. Data Tables **71**, 1 (1999).
[27] H. Ströbele *et al.*, Phys. Rev. C **27**, 1349 (1983).
[28] Y. G. Ma, Phys. Rev. Lett. **83**, 3617 (1999).
[29] A. Bonasera *et al.*, Riv. Nuovo Cimento **23**, 1 (2000).
[30] P. Danielewicz *et al.*, Science **298**, 1592 (2002).
[31] A. Andronic *et al.*, Phys. Lett. B **612**, 173 (2005).
[32] T. Z. Yan *et al.*, Phys. Lett. B **638**, 50 (2006).
[33] S. Voloshin *et al.*, Z. Phys. C **70**, 665 (1996).
[34] D. Brill *et al.*, Z. Phys. A **355**, 61 (1996).
[35] H. H. Gutbrod *et al.*, Phys. Lett. B **216**, 267 (1989).
[36] P. J. Siemens and J. O. Rasmussen, Phys. Rev. Lett. **42**, 880 (1979).
[37] W. Reisdorf *et al.*, Nucl. Phys. A **612**, 493 (1997).